Chapter 6

Beam Elements

6.1 Introduction

The primary aim of this project is to develop an improved assessment procedure for building response to tunnelling by advancing the use of beam elements to represent masonry building facades in numerical models. In this chapter, the beam theories introduced briefly in Chapter 4 are revisited and discussed in detail through a review of the theories and their finite elements in the literature. Timoshenko beam finite elements are chosen for use in this study to represent building facades. A description of their formulation, implementation in to OXFEM (including the new equivalent elastic and masonry beam models) and testing is given in this Chapter. Finally, beam elements representing building facades are subjected to imposed ground displacements their response is compared to the response of the full facades from Chapter 4.

6.2 Literature review

The simplest beam theory is the classical theory known as *Bernoulli-Euler* theory. Under this theory, for a beam with its centroidal axis along the x-axis, of cross sectional area, A, second moment of area (about the y-axis), I, and Young's modulus, E, under the action

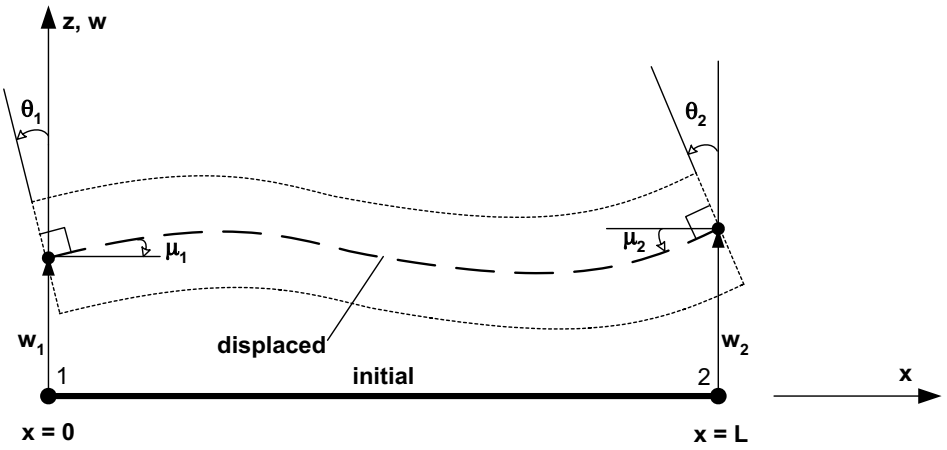

Figure 6.1: **Bernoulli-Euler beam theory (after Astley, 1992)**

of bending moment, M, shear force, Q, and axial force, P, the resulting displacements are $u(x)$ and $w(x)$ in the x and z directions respectively (Astley, 1992). The key assumption for displacements under this theory is that plane sections initially perpendicular to the centroidal axis, remain plane and perpendicular to the axis after deformation. Figure 6.1 shows a beam element based on this theory of length, L, with transverse end displacements, w_1 and w_2, rotation of the end planes θ_1 and θ_2 and rotation of the neutral axis, μ_1 and μ_2 (axial displacements u_1 and u_2 are not shown). The requirement that cross-sections remain perpendicular to the neutral axis means that θ_1 and θ_2 equal μ_1 and μ_2 respectively.

The deflection equation for such a beam can be derived using the fact that $\theta = \mu$ and $\mu = dw/dx$ as described by Timoshenko (1957) and given as

$$\frac{d^2w}{dx^2} = -\frac{M}{EI} \tag{6.1}$$

The strain energy (SE) per unit length (ignoring axial effects) is thus

$$SE/length = \frac{1}{2}EI\left(\frac{d^2w}{dx^2}\right)^2 \tag{6.2}$$

The assumption that plane sections remain perpendicular to the centroidal axis necessarily implies that shear strain, γ_{xz}, is zero. This in turn implies that shear stress and shear force are zero. The only loading case resulting in zero shear force is a constant bending moment,

and thus Bernoulli-Euler theory strictly holds only for this case. As Astley (1992) notes, this formulation ignoring stresses due to shear can also be used for other load cases, but is acceptable only for long slender beams as errors incurred in displacements by ignoring shear effects are of the order of H/L^2, where H is the depth of a beam and L is the length. Where a beam is relatively short or deep, shear effects can, however, be significant (Timoshenko, 1957). As discussed in Chapter 4, it is evident that shear effects are indeed significant in the analysis of building facades and such effects were considered in the derivation of the imposed displacements applied to the facades for this thesis. Shear effects are thus also required in any surface beams used to represent building facades.

An analytical beam theory with shear effects included is the theory known as *deep* or *Timoshenko* beam theory. The critical difference in Timoshenko theory is that the assumption that plane sections remain plane and perpendicular to the neutral axis is relaxed to allow plane sections to undergo a shear strain γ. The plane section still remains plane but rotates by an amount, θ, equal to the rotation of the neutral axis, μ, minus the shear strain γ as shown in figure 6.2. The rotation of the cross section is thus

$$\theta = \mu - \gamma \tag{6.3}$$

which by using $\mu = dw/dx$ leads to

$$\frac{d\theta}{dx} = \frac{d^2w}{dx^2} - \frac{d\gamma}{dx} \tag{6.4}$$

and the beam deflection equation (which replaces equation 6.1) becomes

$$\frac{d\theta}{dx} = -\frac{M}{EI} \tag{6.5}$$

The expression for strain energy in the beam now consists of a bending and a shear term. Timoshenko theory assumes that shear strain is constant over the cross-section. In reality, the shear stress and strain are not uniform over the cross section so a *shear coefficient*, k is introduced as a correction factor to allow the non-uniform shear strain to be expressed as a

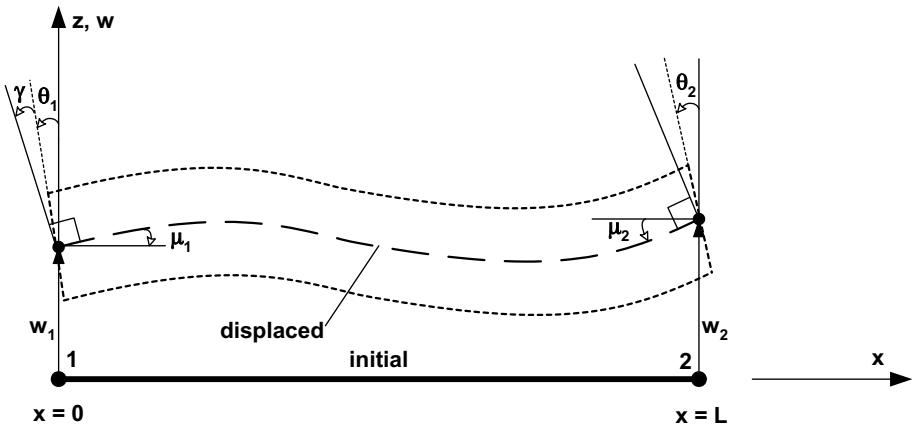

Figure 6.2: **A Timoshenko beam element (after Astley, 1992)**

constant. The shear coefficient approximates the correct integrated value of strain energy due to shear ($1/2\tau\gamma$) as an assumed constant average or centreline value (Astley, 1992). The value of the coefficient depends on the shape of the cross section and was originally introduced by Timoshenko (1921); details regarding its derivation and appropriate values are presented below. Using the shear coefficient, average shear strain is taken as $\gamma = Q/kAG$ and the strain energy per unit length due to bending only thus becomes

$$SE/length = \frac{1}{2}EI\left(\frac{d\theta}{dx}\right)^2 + \frac{1}{2}kAG\gamma^2 \tag{6.6}$$

The Timoshenko theory presented above can be used to develop beam elements which include shear displacements for use in finite element analyses. Numerous different finite element formulations of Timoshenko beams exist and many early types are described by Thomas et al. (1973) including the generally acknowledged starting point for Timoshenko beam development: the McCalley (1963) beams as developed by Archer (1965) with four degrees of freedom comprising w and θ (as defined above and shown in figure 6.2) at each of two nodes. Detailed derivations for the stiffness matrix of the Archer beams are given by Przemieniecki (1968) (who notably neglects to include the shear coefficient) by utilising a displacement formulation. Davis et al. (1972) present a formulation (including the shear coefficient) for the same four degree of freedom element, based on exact static solutions

for equilibrium of a beam with forces and moments applied only at the nodes. This leads to shear force being constant along the beam. The lateral deflection is a cubic polynomial function of x and the cross sectional rotation is a dependent quadratic function. Additional discussion of both this element and the use of various interpolation functions is given below.

A large number of other two node Timoshenko beam formulations exist in the literature, but as noted by Narayanaswami and Adelman (1974), Dawe (1978) and others, some confusion exists regarding the appropriate rotational degree of freedom to be used at the nodes. In some cases, the shear strain has been used (Thomas et al., 1973), in others the value of dw/dx (Severn, 1970 and Nickel and Secor, 1972) as well as various combinations of cross section rotation θ, shear strain and dw/dx. As Dawe (1978) and Davis et al. (1972) point out: the correct rotational degree of freedom is the cross sectional rotation, θ; the use of dw/dx does not enable the clamped end boundary condition to be represented correctly.

Higher order Timoshenko beams, having more than four degrees of freedom, also exist in the literature. Kapur (1966) develops a beam element by considering shear and bending displacements separately, with a cubic displacement function assumed for both the bending and the shear deformation. A translational and a rotational degree of freedom is introduced at each node for both bending and shear leading to a two node, eight degree of freedom element. Davis et al. (1972) criticise the Kapur beam for its inability to couple forces and displacements correctly when adjacent elements are not colinear, due to the separation of bending and shear. In their beam discussed above, shear force is the first derivative of bending moment thus coupling bending and shear and eliminating the need for the additional degrees of freedom of Kapur (1966). Nickel and Secor (1972) propose an element with seven degrees of freedom which include w, dw/dx and θ at each of two end nodes and θ at an additional mid-element node with a cubic function for w and a quartic function for θ. Dawe (1978) presents an element with three nodes, each of which has degrees of freedom of w and θ leading to a coupled situation with a quintic variation of w and a quartic variation of θ. Dawe concludes that the approach coupling the correct primary variables (w and θ), is superior to an approach where independent functions are assumed as it leads to considerably fewer degrees of freedom being required for a given order of

interpolation.

Higher order elements have also been developed by Levinson (1981) and Heyliger and Reddy (1988) that account for the true shear stress distribution throughout the beam cross section and removes the need to use Timoshenko's shear coefficient. The higher order shear stress distribution means that the Timoshenko assumption of cross sections remaining plane is relaxed to allow warping into a non-planar surface.

Timoshenko beam elements with low order interpolation functions can exhibit a very stiff response as the beams become very thin. This phenomenon is known as *shear locking* and is a result of inconsistencies in interpolation functions used for w and θ. Beam elements with linear interpolation for both these variables are particularly susceptible (Reddy, 1997). To overcome locking a number of techniques are proposed including reduced order integration (Prathap and Bhashyam, 1982). Reddy (1997)(three-nodes) and Kosamtka (1994)(two-nodes) give a number of examples of formulations with different order interpolations in his development of locking-free Timoshenko beam elements. An approach to choosing appropriate interpolation functions for beam elements using Hermitian and Lagrange polynomials is presented by Augarde (1997) and is discussed in section 6.4.1.

The shear coefficient, k, was introduced by Timoshenko (1921 and 1922) as a correction factor (originally denoted λ, where $\lambda = 1/k$) to be applied to the average shear stress and shear strain to obtain centreline values to be used in the beam theory. In his original introduction of the theory, Timoshenko gave the shear correction factor the value of 2/3 for rectangular beams, with the value depending on the shape of the cross section. As Levinson (1981) notes, from its inception, the calculation of the 'best' shear coefficient has become in itself a 'small research industry' with much debate over the appropriate definition and derivation of the value. The most generally well regarded and widely used values are due to Cowper (1966) who clarifies the original definition and derives, using three-dimensional elasticity theory, a new formula to calculate k values for any cross section. Cowper (1966) tabulates standard formulae for a variety of cross sections and for a standard rectangular

cross section gives the formula including ν, the Poisson's ratio for the material as

$$k = \frac{10\,(1+\nu)}{12+11\nu} \tag{6.7}$$

Throughout the early development of Timoshenko beams, only straight elements were considered. Curved beams have, however, also been developed and are useful in analysing curved structural elements such as tunnel linings. Curved beams suffered from *membrane locking*, a phenomenon similar to the shear locking described above for straight beams. Attempts at formulating locking-free curved beam elements include those of Ramesh Babu and Prathap (1986) with two nodes and linear interpolation for all variables, and Prathap and Ramesh Babu (1986) with three nodes and quadratic interpolation. Both these formulations suffer from locking and errors due to lack of consistency between shear and membrane fields caused by poor choice of nodal degrees of freedom. Day and Potts (1990) attack this problem by utilising Mindlin plate theory (for the inclusion of shear deformation in plate elements) to develop shear capable curved beams for modelling structural components in plane strain finite element analyses. Here the plane strain versions of the Mindlin three-dimensional plate equations (as described by Zienkiewicz (1997) and Astley (1992) among others) are used by Day and Potts to formulate locking and error free curved plain strain (and axi-symmetric) beam elements. In particular, they note and clarify the confusion in the literature regarding the appropriate nodal degrees of freedom to use. Potts and Zdravkovic (1999 and 2001) give a good description of the Mindlin beam formulation and its use for two-dimensional analyses. Such beams are also used by Potts and Addenbrooke (1997) to represent buildings in plane strain in their work on the relative stiffness method for soil-structure interaction in tunnelling described in Chapter 2.

Another approach to including shear effects is the use of *hybrid* beams as described by Bakker (2000). Here, the necessity for shear flexibility is provided, but rotational degrees of freedom are condensed out of the beam elements by replacing the requirement for continuity of rotations with continuity of bending moments between adjacent beam elements. Another beam developed without rotational degrees of freedom is the overlapping formulation of Phaal and Calladine (1992) used by Augarde (1997) for tunnel lining elements. In this

approach each node acts as the centre node of one element and the end node of two other elements with each element overlapping two others. This overlapping provides continuity of slope without the need for rotational degrees of freedom.

6.3 Choice of appropriate beam element

The beam elements chosen for use in this study are based on the straight two node beam elements first described by Davis et al. (1972); the similar and more recent description of the formulation of these beams by Astley (1992), however, will be followed here.

The primary task for the beams in this research is the representation of building facades which are generally considered to be straight or able to be represented by a combination of straight sections. This removes a need for curved beam elements. It is also considered that higher order beams with more than two nodes are not required. The use of higher order beams would introduce greater incompatibility of displacements between beam and soil elements away from the nodes, as is discussed below. Higher order beams accounting for the true stress and strain distribution through a cross-section are also not required, with the Timoshenko approach to including shear considered adequate.

The aim of this thesis is to expand beam element representations of buildings into three dimensions. This means that plane strain beam formulations such as the Mindlin beams described above, which are excellent for use representing long structures such as tunnel linings or retaining walls in plane strain but cannot be used for a discreet structure above a tunnel in three dimensions, will not be adequate for this study. Fully three-dimensional beam elements (often known as *frame* elements) are thus required; the capabilities for bending deformation in two planes, axial deformation and torsion about their own axis are all necessary. Such beams need to be able to be located anywhere in three-dimensional space. The Timoshenko theory described above for a simple two node plane beam with no axial effects is therefore expanded for use in formulating such three-dimensional elements.

This research aims to represent facades as equivalent beams on the surface. A recent

approach to modelling masonry facades as equivalent frame systems, comprised of beams arranged in a grid was recently described by Roca et al. (2005). This is an intermediate approach between the full modelling of masonry facades and the use of surface beams.

From the analysis in Chapter 4, the necessity to independantly specify shear (GA) and bending (EI) rigidities for beam elements representing a building facades was made clear. The beam element formulation for this study is chosen to enable such specification. Notably, this has not historically been possible in some popular commercial finite element codes. The version of ABAQUS available at the start of this research (version 5.8, released 1998), contained Timoshenko beam elements that could be used in plane or 3D analyses, but did not allow separate specification of EI and GA; the shear rigidity was simply assumed to be half the bending rigidity. This would be unacceptable for use on this project, given the newly developed methods of determining beam properties with un-linked rigidity values. By late 2002, after this research was underway, a new version of ABAQUS (version 6.3, released September 2002) included the facility for the user to specify independent values for shear and bending rigidity, indicating that the software developers had also decided that independent specification of these properties was a useful attribute.

6.4 Formulation of Timoshenko beam elements

The beam element implemented is shown in figure 6.3. It is straight with six degrees of freedom at each node, three translations and three rotations. The formulation of the element stiffness matrix for this beam comprises contributions from four separate actions: one axial, one torsional and two bending, one about each of two orthogonal local axes. The contributions from axial and torsional effects to the element stiffness are formulated in the conventional manner and are detailed in Appendix B. The bending contributions to the stiffness matrix assume Timoshenko beam theory as described above. The contribution of bending in each orthogonal direction can be considered independently as the principal axes of the beam are chosen to coincide with the local x-y and x-z planes (Przemieniecki, 1968). These are denoted the *out-of-plane* and *in-plane* directions respectively.

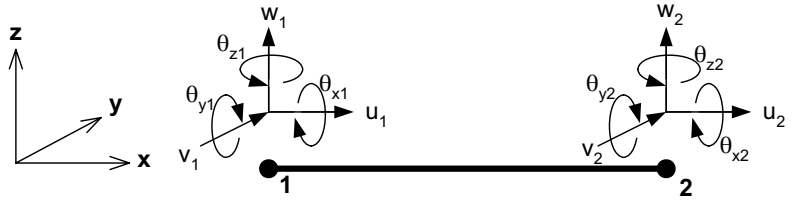

Figure 6.3: **Beam element for three-dimensional analyses**

6.4.1 Interpolation functions

In this section the bending shape functions in the x-z plane are formulated. The derivation, based on Astley (1992), follows the common convention (used by Augarde (1997) in the original formulation of Bernoulli-Euler beams in OXFEM) of formulating the shape functions in terms of the non-dimensional variable $\bar{x}$ where

$$\bar{x} = \frac{x}{L} \tag{6.8}$$

with element length, L, such that the two-node beam has nodes at $\bar{x} = 0$ and 1. As for a two-node Bernoulli-Euler beam element, the lateral displacement, $w(\bar{x})$, is expressed as

$$w(\bar{x}) = N_1(\bar{x})w_1 + N_2(\bar{x})\mu_1 + N_3(\bar{x})w_2 + N_4(\bar{x})\mu_2 \tag{6.9}$$

where $N_i(\bar{x})$ are shape functions associated with the displacements (w) and rotations (μ) at the nodes. For a Timoshenko beam, however, we must also include variation for shear, γ. The simplest approach, from Astley (1992), is to assume that γ is a constant equal to γ_0. This zeroth order interpolation therefore assumes a constant shear stress and shear force within each element. As γ_0 is an independent variable, the element thus has a fifth degree of freedom in bending. Rewriting the expression for lateral displacement using equation 5.3 to replace μ in terms of θ and γ_0 thus gives

$$w(\bar{x}) = N_1(\bar{x})w_1 + N_2(\bar{x})(\theta_1 + \gamma_0) + N_3(\bar{x})w_2 + N_4(\bar{x})(\theta_2 + \gamma_0) \tag{6.10}$$

which upon rearranging leads to

$$w(\bar{x}) = N_1(\bar{x})w_1 + N_2(\bar{x})\theta_1 + N_3(\bar{x})w_2 + N_4(\bar{x})\theta_2 + N_5(\bar{x})\gamma_0 \tag{6.11}$$

where $N_5(\bar{x}) = N_2(\bar{x}) + N_4(\bar{x})$. In standard matrix form this reduces to

$$w(\bar{x}) = \boldsymbol{N_b^e d_{b\gamma}^e} \tag{6.12}$$

where the bending shape functions and degrees of freedom for an element are respectively

$$\boldsymbol{N_b^e} = \{N_1 \;\; N_2 \;\; N_3 \;\; N_4 \;\; N_5\} \tag{6.13}$$

$$\boldsymbol{d_{b\gamma}^e} = \{w_1 \;\; \theta_1 \;\; w_2 \;\; \theta_2 \;\; \gamma_0\}^T \tag{6.14}$$

The shape functions N_i are generated by the method described by Augarde (1997) using Hermitian interpolating polynomials. Hermitian interpolation involves the use of both an expression for ordinate information at known points and its derivative to determine approximate values between known locations (Cook et al., 1989). Augarde notes that for beam elements, the requirements for shape functions satisfy the definition of Hermite polynomials as the rotations can be considered as the first derivatives of the lateral displacements under the assumption of small displacement theory. These Hermite polynomials can be derived from Lagrange polynomials. This is particularly useful for developing finite element programs, as Lagrange polynomials are used for the shape functions for continuum elements and the axial effects in beam elements, and are thus already in the program code.

For beam elements, one-dimensional interpolation is required along the element centreline necessitating the use of one-dimensional Hermite polynomials. These can be obtained directly from Langrange polynomials using

$$H_{0i}^1 = [1 - 2(x - x_i)L_i'(\bar{x}_i)][L_i(\bar{x})]^2 \tag{6.15}$$

$$H_{1i}^1 = (x - x_i)[L_i(\bar{x})]^2 \tag{6.16}$$

where H_{ji}^r is a Hermite polynomial of level r and derivative order j at node i. The level of the Hermite polynomial indicates the highest order derivative used in the interpolation. $L_i(\bar{x})$ is the one dimensional Lagrange interpolating polynomial of degree $(n-1)$

$$L_i(\bar{x}) = \prod_{j=1, j\neq i}^{n} \frac{x - x_i}{x_i - x_j} \tag{6.17}$$

and $L_i'(\bar{x})$ is the first derivative. The derivations of the particular interpolating polynomials for the shape functions $N_1(\bar{x})$ to $N_4(\bar{x})$ for the Timoshenko beam being implemented here are given in Appendix B.

6.4.2 Formation of element stiffness matrix

Assembly of the bending contribution to the element local stiffness matrix including the shear degree of freedom follows the conventional method. As is usual for beam elements, the strain-displacement matrix $\boldsymbol{B}$, is used such that the product $\boldsymbol{Bd}$ gives beam curvatures. The strain-displacement matrix relationship is thus $\boldsymbol{B} = d^2\boldsymbol{N}/dx^2$, the use of which gives

$$\boldsymbol{B_b^e} = \frac{1}{L^2}\left[\begin{array}{ccccc} N_1''(\bar{x}) & N_2''(\bar{x}) & N_3''(\bar{x}) & N_4''(\bar{x}) & N_5''(\bar{x}) \end{array}\right] \tag{6.18}$$

where $\boldsymbol{B_b^e}$ is the strain-displacement matrix for an element in bending and $N_i''(\bar{x})$ are the second derivatives with respect to $\bar{x}$ of the bending shape functions (from Appendix B).

The local element stiffness matrix including the shear degree of freedom, $\boldsymbol{K_{b\gamma}^e}$, is thus formed in the usual manner using

$$\boldsymbol{K_{b\gamma}^e} = L\int_0^1 \boldsymbol{B_b^{eT}}\boldsymbol{D}\boldsymbol{B_b^e}d\bar{x} \tag{6.19}$$

where $\boldsymbol{D}$ is the material property matrix, including EI, with Young's modulus E and second moment of area I and kGA with shear coefficient k, shear modulus G and cross-

sectional area A. This leads to

$$\boldsymbol{K}^{\boldsymbol{e}}_{\boldsymbol{b\gamma}} = \begin{bmatrix} 12a & 6aL & -12a & 6aL & 12aL \\ 6aL & 4aL^2 & -6aL & -2aL^2 & 6aL^2 \\ -12a & -6aL & 12a & -6aL & -12aL \\ 6aL & 2aL^2 & -6aL & 4aL^2 & 6aL^2 \\ 12aL & 6aL^2 & -12aL & 6aL^2 & (12aL^2+b) \end{bmatrix} \tag{6.20}$$

where $a = EI/L^3$ and $b = kGAL$.

The orthogonal plane in bending gives an identical stiffness contribution but in the second plane, assuming, as described above, that the *out-of-plane* and *in-plane* directions coincide with the principal directions of bending. Summing of the contributions of the two bending planes, the axial and the torsional effects leads to a 14×14 local element stiffness matrix, $\boldsymbol{K}^{\boldsymbol{e}}_{\boldsymbol{\gamma}}$, including the shear terms. A Timoshenko beam element formulated in this manner with 14 degrees of freedom, could not be used in place of a Bernoulli-Euler theory based frame element which would have only 12 degrees of freedom, without renumbering and modifying the surrounding mesh to accommodate the extra degrees of freedom (Astley, 1992). It is thus common practice to condense out the extra two shear degrees of freedom.

For each of the individual 5×5 bending stiffness matrices including shear, the condensation process involves extracting out the shear row of the matrix and solving for the constant shear strain γ_0. This is a simple process as γ_0 is unique to each element, and is only connected to the four other members of the array of bending degrees of freedom $\boldsymbol{d}^{\boldsymbol{e}}_{\boldsymbol{b\gamma}}$. If we assume that loads are applied only at the nodal points, there would be no forces appearing in the force-displacement equation formed using the γ_0 row of the stiffness matrix. Solving for the constant shear strain under this assumption thus gives

$$\gamma_0 = \frac{1}{12aL^2+b}\left[-(12aL)w_1 - (6aL^2)\theta_1 + (12aL)w_2 - (6aL^2)\theta_2\right] \tag{6.21}$$

If we let $c = 6aL/(12aL^2+b)$, the relationship between the degrees of freedom can be

expressed as

$$\begin{Bmatrix} w_1 \\ \theta_1 \\ w_2 \\ \theta_2 \\ \gamma_0 \end{Bmatrix} = \begin{bmatrix} 1 & 0 & 0 & 0 \\ 0 & 1 & 0 & 0 \\ 0 & 0 & 1 & 0 \\ 0 & 0 & 0 & 1 \\ -2c & -cL & 2c & -cL \end{bmatrix} \begin{Bmatrix} w_1 \\ \theta_1 \\ w_2 \\ \theta_2 \end{Bmatrix} \tag{6.22}$$

or in matrix notation

$$\boldsymbol{d}^{\boldsymbol{e}}_{\boldsymbol{b\gamma}} = \boldsymbol{T}_{\boldsymbol{b}} \boldsymbol{d}^{\boldsymbol{e}}_{\boldsymbol{b}} \tag{6.23}$$

The condensed stiffness matrix for bending in one plane is thus

$$\boldsymbol{K}^{\boldsymbol{e}}_{\boldsymbol{b}} = \boldsymbol{T}_{\boldsymbol{b}}{}^{T} \boldsymbol{K}^{\boldsymbol{e}}_{\boldsymbol{b\gamma}} \boldsymbol{T}_{\boldsymbol{b}} \tag{6.24}$$

In the formulation implemented into OXFEM, this condensation operation is performed on the full 14×14 matrix making use of an expanded condensation matrix, $\boldsymbol{T}$, yielding a 12×12 element local stiffness matrix. Transforming the local element stiffness matrix for the beams oriented in three dimensional space to a global element stiffness matrix for assembly and solution in the global domain is by the conventional method of pre and post-multiplication by a transformation matrix comprising direction cosines derived from the global coordinates of the element nodes.

The determination of the stiffness matrix in OXFEM is by one-dimensional Gaussian quadrature. With the shape functions including terms of order three and below and the $\boldsymbol{B}$ matrix containing terms of order one or lower, the solution for the stiffness matrix is given exactly by two-point Gauss quadrature.

6.4.3 Compatibility of elements

The Timoshenko beams implemented as described above are for use in conjunction with ten-noded tetrahedral continuum elements to model the ground. The two-noded surface beams will therefore lie two to an edge of a tetrahedron at the ground surface. Displacements interpolated between the nodes of the beam elements will differ from those along the edge of the continuum element. The different element types therefore exhibit incompatible displacements at locations other than nodal points, but compatible displacements at each node. This incompatibility results from the transverse displacement of the beam elements being described by a cubic interpolation function (the beam nodes having four contributing degrees of freedom: two rotations and two displacements) while the displacement along an edge of a soil element is described by a quadratic function (as there are three nodes each with one displacement degree of freedom).

The amount of lack of conformity (as measured by the difference in strain energy due to transverse displacements) introduced by the arrangement of having two two-noded Timoshenko beams meeting a 10-noded tetrahedral soil element side is lower than if Timoshenko beams with three nodes (two end nodes and a mid-side node) were to be used. It is, however, higher than if the two-noded Timoshenko beams were used in conjunction with 20-noded tetrahedral soil elements. The use of these soil elements, however, would lead to unnecessarily long run times for analyses due to the additional degrees of freedom. Ten-noded tetrahedra are thus used for the soil. The incompatibility of the chosen soil and beam elements away from the nodal points is not considered to introduce significant detrimental effects as long as element lengths are kept sensibly short at locations where the two element types meet.

6.4.4 Constitutive models and stress updating

The two constitutive models introduced in Chapter 4 are for use with the Timoshenko beam elements. The *equivalent elastic beam* model is linearly elastic with beam properties described in section 4.3 and is formulated in OXFEM in the conventional manner. The

equivalent masonry beam model, however, is non-linear as described in section 5.4. The in-plane bending rigidity is dependent on the direction (hogging or sagging) and magnitude of the curvature of the beam. When using this constitutive model, the assignment of beam properties and stress resultant (moment) updating following solution for the displacements becomes more complex.

The solution techniques used in the OXFEM finite element code are fully described in section 7.5, however it is useful to briefly describe the approach adopted for the Timoshenko beams here. For non-linear material, a Modified Euler solution scheme is used in OXFEM where loading is applied incrementally. For each incremental step, the stiffness matrix for a Timoshenko beam element is dependent on the strain after the previous increment. The current bending strains are thus used to calculate the in-plane bending rigidity at each step according to equation 5.7 prior to the solution of displacements.

Following solution for displacements at each step, updating of strains and stresses takes place. Strains, $\boldsymbol{\epsilon}$, at a beam node are updated incrementally according to

$$\boldsymbol{\epsilon^i} = \boldsymbol{\epsilon^{(i-1)}} + \boldsymbol{B}\Delta\boldsymbol{d} \tag{6.25}$$

where i is the current step number and $\boldsymbol{d}$ are the nodal displacements.

Stress updating for the Timoshenko beams is done on a total stress basis. Instead of the incremental approach adopted for other non-linear materials in OXFEM where

$$\boldsymbol{\sigma^i} = \boldsymbol{\sigma^{(i-1)}} + \boldsymbol{D}\Delta\boldsymbol{\epsilon} \tag{6.26}$$

the approach adopted for the Timoshenko beams makes use of the explicit total stress-strain relationship. For the non-linear relationship for in-plane bending, equation 5.6 is used to give the bending stress (moment) using the already updated current strain.

6.5 Implementation and testing of Timoshenko beams in OXFEM

The Timoshenko beams as described above were implemented into the OXFEM finite element program. This involved both the inclusion of new FORTRAN 90 code and the updating and amending of many existing subroutines within the program. Once implemented, testing and validation of the Timoshenko beam elements were undertaken. Validation of the Timoshenko beams included the following test problems, shown in figure 6.4, undertaken with beams with elastic properties except where noted:

1. Plane simply supported beam with mid-span point load;
2. Simply supported beam in three-dimensional space with multiple orthogonal mid-span point loads;
3. Plane cantilever beam with point load;
4. Plane simply supported beam with distributed load;
5. String of beams on an elastic soil;
6. Footing of beams on an elastic soil; and
7. Plane simply supported beam with equivalent masonry properties with distributed load.

For the first three test problems the finite element results for displacement under the point load exactly match the analytical answers (using Timoshenko beam theory) using only one element in problem 3 and two elements in each of problems 1 and 2. This is to be expected as the order of the interpolating polynomial for transverse displacement matches the order of the expression for the transverse displacement field for these problems, both being cubic functions. The input parameters and solutions to these tests are given in table 6.1.

For test problem 4, the finite element analysis does not provide an exact solution (as the order of the displacement function is higher than the order of the interpolating polynomial),

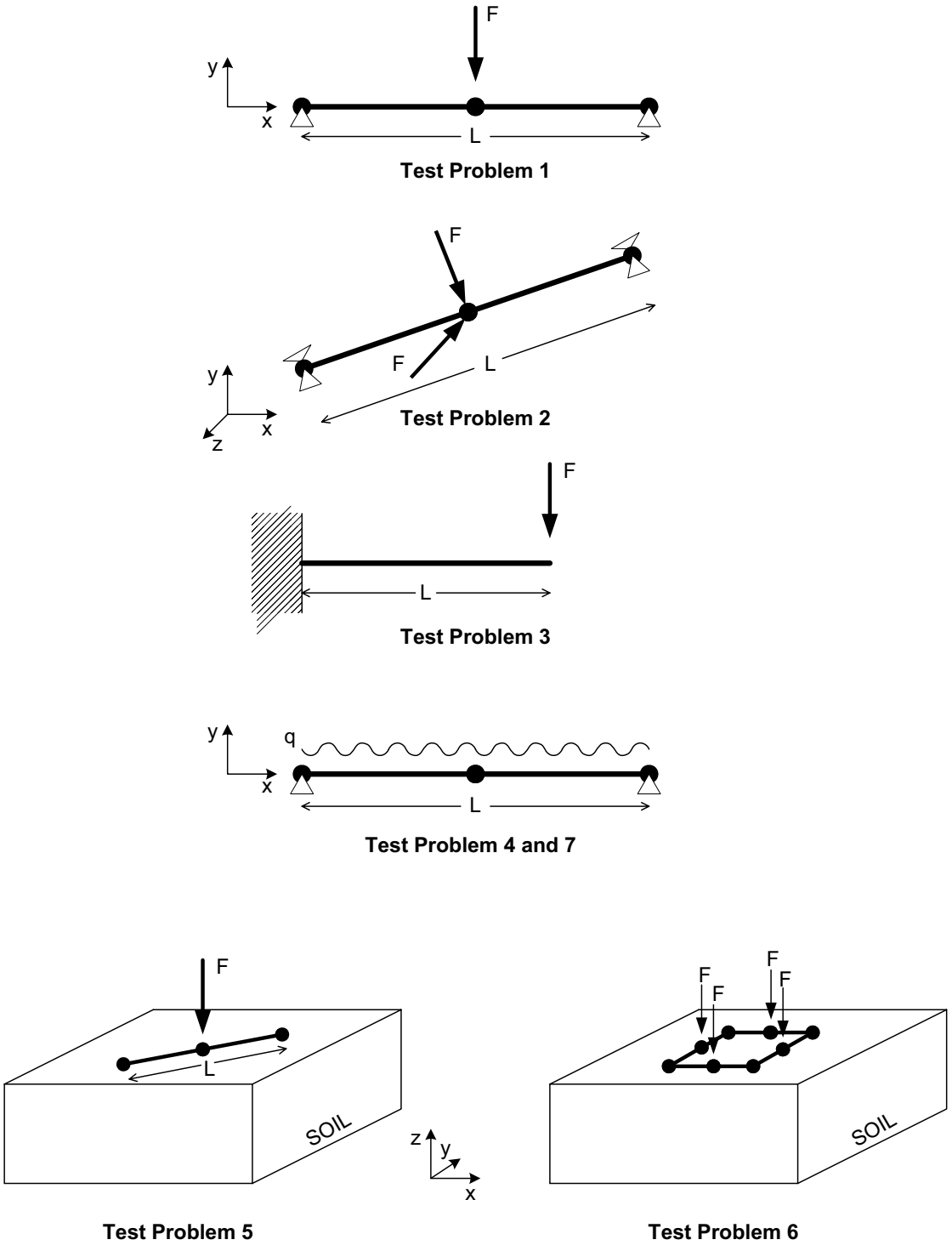

Figure 6.4: **Test problems for validation of Timoshenko beam elements**

Table 6.1: **Timoshenko beam test problems**

Test Problem1: Input Parameters			
A	**L**	**I**	**J**
7240mm^2	3000mm	$1.610 \times 10^8\text{mm}^4$	$3.380 \times 10^5\text{mm}^4$
E	**G**	**k**	**F**
$2.000 \times 10^5\text{MPa}$	$8.000 \times 10^4\text{MPa}$	0.667	$1.000 \times 10^6\text{N}$

Test Problem 1: Results		
Analytical Expression	Analytical Result	FE Result
$v_y = \frac{PL^3}{48EI} + \frac{PL}{4kAG}$	19.411mm	19.411mm

Test Problem 2: Input Parameters (both in-plane and out-of-plane)			
A	**L**	**I**	**J**
7240mm^2	3000mm	$1.610 \times 10^8\text{mm}^4$	$3.380 \times 10^5\text{mm}^4$
E	**G**	**k**	**F**
$2.000 \times 10^5\text{MPa}$	$8.000 \times 10^4\text{MPa}$	0.667	$1.000 \times 10^6\text{N}$

Test Problem 2: Results		
Analytical Expression	Analytical Result (v_y and w_z)	FE Result (v_y and w_z)
$v_y = w_z = \frac{PL^3}{48EI} + \frac{PL}{4kAG}$	19.411mm	19.411mm

Test Problem 3: Input Parameters			
A	**L**	**I**	**J**
7240mm^2	1000mm	$1.610 \times 10^8\text{mm}^4$	$3.380 \times 10^5\text{mm}^4$
E	**G**	**k**	**F**
$2.000 \times 10^5\text{MPa}$	$8.000 \times 10^4\text{MPa}$	0.667	$1.000 \times 10^6\text{N}$

Test Problem 3: Results		
Analytical Expression	Analytical Result	FE Result
$v_y = \frac{PL^3}{3EI} + \frac{PL}{kAG}$	12.942mm	12.942mm

Test Problem 4: Input Parameters			
A	**L**	**I**	**J**
7240mm^2	3600mm	$1.610 \times 10^8\text{mm}^4$	$3.380 \times 10^5\text{mm}^4$
E	**G**	**k**	**q**
$2.000 \times 10^5\text{MPa}$	$8.000 \times 10^4\text{MPa}$	0.667	$3.000 \times 10^2\text{N/mm}$

Test Problem 4: Results	
Analytical Expression	Analytical Result
$v_y = \frac{qL^4}{384EI} + \frac{qL^2}{8kAG}$	21.634mm

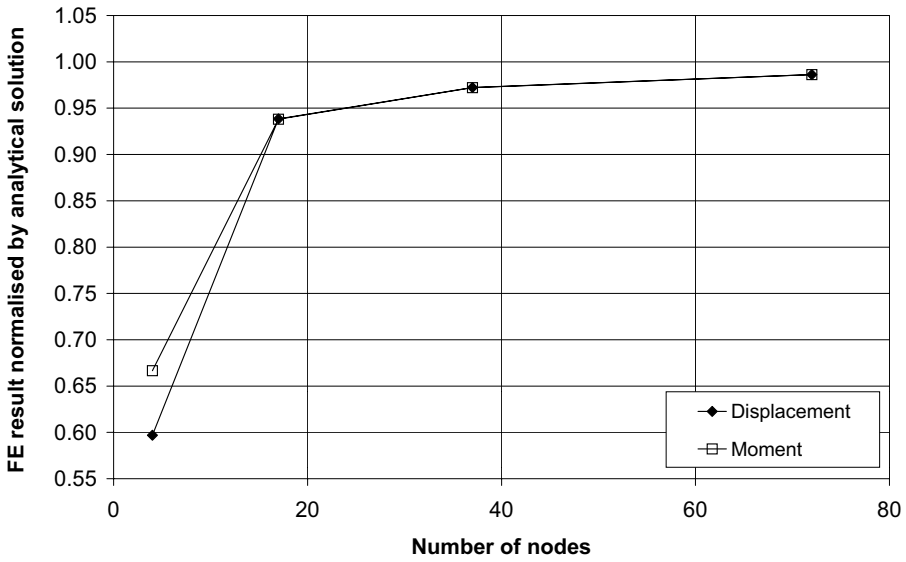

Figure 6.5: **Convergence of finite element result and analytical solution for test problem 4**

but converges to the analytical solution with increasing mesh density. Table 6.1 gives the input parameters and analytical solution for this test while the convergence of the finite element results to the analytical solution with increasingly finer meshes is shown in figure 6.5. Convergence to within 2% of the analytical solution occurs for meshes with approximately 50 nodes and to within 1.4% for meshes with 70 nodes.

There appears to be no precise analytical solution to the problem in test 5 for a Timoshenko beam on elastic soil. A comparison was thus made between the beam displacement for this test using OXFEM and the displacement calculated by the program ABAQUS for the same test. The input parameters for the Timoshenko beams and the elastic soil as well as the results are given in table 6.2. Linear elastic soil and elastic Timoshenko beam elements were specified in each program. The Timoshenko beam formulations were similar, with independent specification of bending and shear properties. The displacements under the point load at the centre of the beam using the two programs were within 0.75%.

Problem 6 was also analysed by comparing the finite element results obtained using OXFEM and ABAQUS. The beam and soil properties as well as the load magnitudes are identical to those given for test problem 5. The sides of the square footing were all 3.0m long and

Table 6.2: **Timoshenko beam test problem 5**

Beam Input Parameters			
A	**L**	**I**	**J**
7240mm^2	3000mm	$1.610 \times 10^8\text{mm}^4$	$3.380 \times 10^5\text{mm}^4$
E	**G**	**k**	**F**
$2.000 \times 10^5\text{MPa}$	$8.000 \times 10^4\text{MPa}$	0.85	$1.000 \times 10^6\text{N}$
Soil Input Parameters			
E	**G**	ν	**Dimensions**
$1.000 \times 10^5\text{kPa}$	$3.356 \times 10^4\text{kPa}$	0.49	$6.0 \times 6.0 \times 3.0\text{m}$
Midpoint Displacement Results			
OXFEM		**ABAQUS**	
5.585mm		5.543mm	

the footing was centred on the surface of the soil block which had the same dimensions as test 5. Midside vertical displacements under the point loads for OXFEM and ABAQUS were 5.43mm and 5.39mm respectively (a difference of 0.8%). The vertical displacements of the corner nodes were 2.40mm and 2.42mm respectively (also a difference of 0.8%).

The final test, problem 7, verifies the implementation of the non-linear constitutive model for the Timoshenko beams. It is a repeat of test 4, undertaken with 72 beam elements, but with equivalent masonry beams rather than elastic. Two tests were undertaken: test 7a where the equivalent masonry beam constitutive model described in section 5.4.3 is used; and test 7b using the alternative model as described in section 5.4.4.

The masonry properties for test 7a are, $\kappa_{crit} = 1.0 \times 10^{-2}$, and $f_b = 0.1$ with other properties and loads for the test the same as in table 6.1 for test 4. Figure 6.6 shows the moment-curvature relationship for test 7a at the central node of the beam under a uniform load causing hogging applied over 10 incremental load steps. It also shows a theoretical bi-linear moment-curvature relationship, with no gradual reduction of stiffness for comparison. The flexural rigidity of the beam reduces as the hogging curvature develops as expected.

The masonry properties for test 7b are, $\kappa_{crit} = -1.5 \times 10^{-2}$, $f_b = 0.1$, $E_B = 2.0 \times 10^3$, the load applied is 30N/mm and other properties are the same as in table 6.1 for test 4. Figure 6.7 shows the moment curvature relationship for test 7b, at the central node of

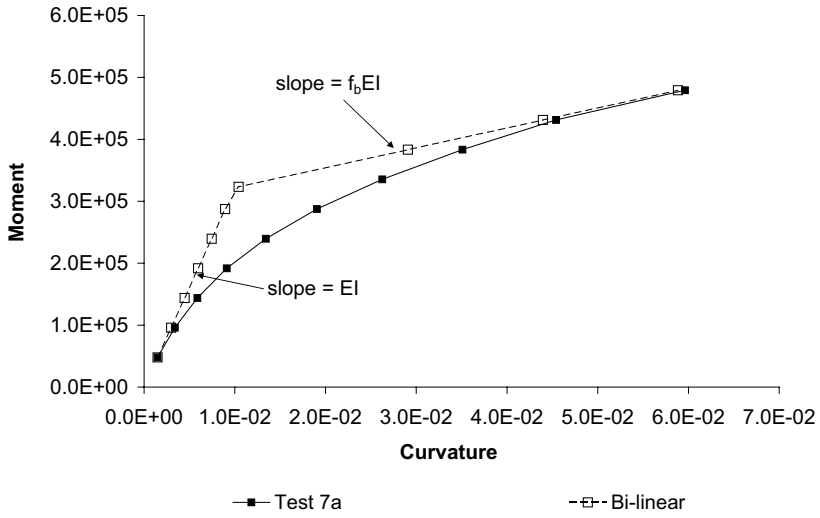

Figure 6.6: **Test 7a: Beam response with equivalent masonry beams**

the beam under a uniform load causing sagging that is applied over 100 incremental load steps. It also shows a bi-linear moment-curvature relationship, with no gradual increase of stiffness for comparison as well as the theoretical moment-curvature relationship if loading had continued beyond the 100 steps. The flexural rigidity of the beam increases as the sagging curvature develops as expected.

Following these problems it was concluded that the 12-degree of freedom Timoshenko beams were successfully implemented in OXFEM.

6.6 Finite element analyses with beam elements

As a more substantial check (before full 3D tunnelling analyses) of the performance of the beam elements and the robustness of the methods developed in Chapter 4 for assigning properties to the beams, a number of 2D analyses are undertaken. The applied displacement analyses of the elastic facades in Chapter 4 are repeated here with the facades replaced with beam elements and the results compared to the full facade analyses. In addition, new analyses with Gaussian displacements are described where the response of a facade and beams are compared. The beam element properties are determined using the equivalent beam methods developed in Chapter 4.

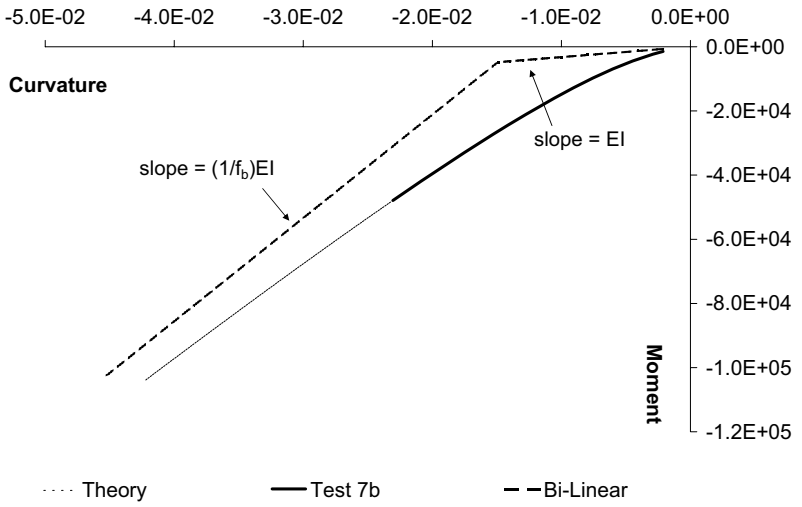

Figure 6.7: **Test 7b: Beam response with alternative equivalent masonry beams**

6.6.1 Beams elements with imposed displacement

The finite element analyses undertaken here involve applying the displacement described by equation 4.5 in sagging to a building with a smooth base. For these analyses, the building facade is represented by a string of elastic Timoshenko beam elements running between the nodes along the base of the facade, rather than the full facade. For these test problems only the in-plane, two-dimensional response of the beams is considered.

For each of the facades noted in table 4.2 and shown in Appendix A, the properties for the beams used here to represent them are determined by applying the *equivalent elastic beam* method described in section 4.3. This provides the effective cross sectional area A^* and second moment of area I^* given in table 4.3 for facades with a smooth base. The Young's modulus, E, and shear modulus, G, for the beams are the same as for the elastic facades. The shear coefficient chosen is Timoshenko's original value of $k = 2/3$ for consistency with the value used in the derivation of the displacement in equation 4.5.

As discussed in section 4.2.5, the output from OXFEM at nodal points is in terms of forces and displacements. To determine the equivalent stress along the base of the beams a similar approach to section 4.2.5 is adopted, however as the beams are two-noded, the nodal forces equivalent to a distributed load on the element differ from those shown in figure 4.7 for the

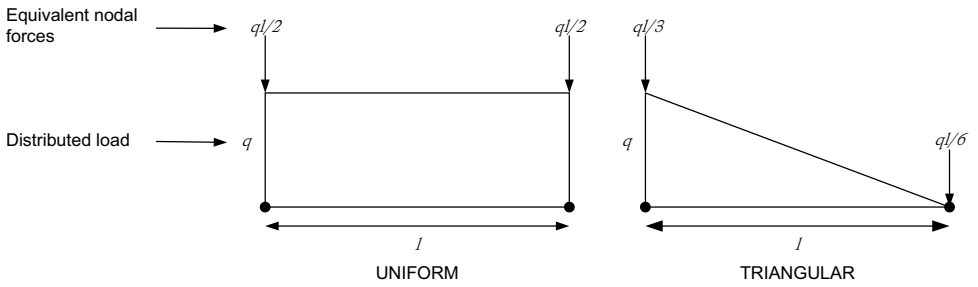

Figure 6.8: **Nodal forces equivalent to distributed loads for beam elements**

three-noded side of a facade element. For a two-noded beam the equivalent nodal forces for a uniformly and linearly distributed load are given in figure 6.8 (Cook et al., 1989), which are used to derive an expression similar to equation 4.6 for the beams.

The results of the finite element analyses are shown in figure 6.9. This figure compares the normalised stiffness ratio (NSR) for the finite element analyses of the beams (K_{febeam}/K_{beam}) with the previously detailed (in figure 4.16) NSR for the facade analyses (K_{fe}/K_{beam}) with the same applied displacement. The labels for the facade and beam families presented in each sub-figure refer to those given in table 4.2 and Appendix A.

It can be seen that the response of the full facades as characterised by the NSR is replicated reasonably well in the analyses with the Timoshenko beams. The agreement is particularly good for facades with no openings, for all values of L/H, with the observed NSR of the beams closely matching the NSR of the facades and reducing for the tests with low L/H as expected. The trend evident in the facade analyses whereby the increasing amount of windows reduces the stiffness of the facades is also replicated in the beam analyses, with the NSR reducing as the amount of windows increases in the facade that the beam represents. The beams, however appear to react more stiffly than the facades for these analyses with a high percentage of openings. The NSRs for the beams in these analyses can be seen to be higher than those of the facades. The reason for this is that the equivalent properties applied to the beams result in them having a slightly higher stiffness than the facades. This is evident in figure 4.17 and is discussed in section 4.3.3.

Overall the results indicate that the beams with properties assigned using the equivalent elastic beam method replicate the response of the facades to an applied displacement

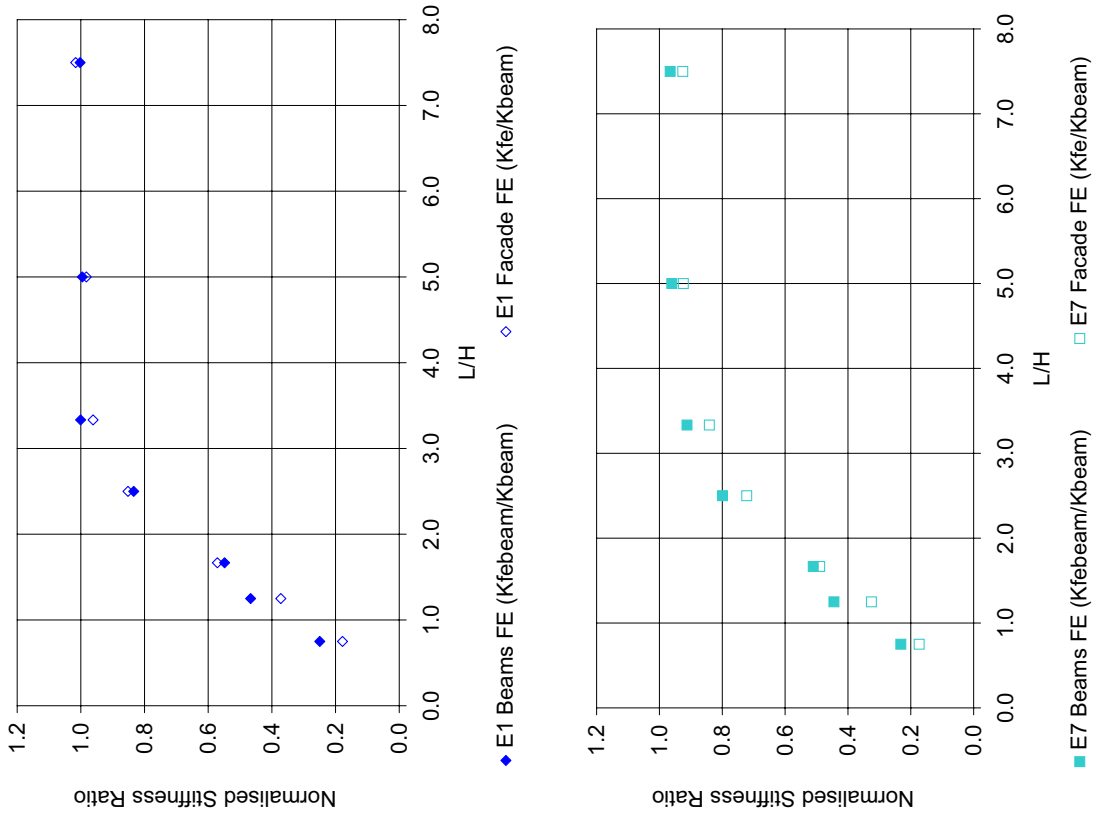

(a) Models E1 - No Windows

(b) Models E7 - 5.625% Windows

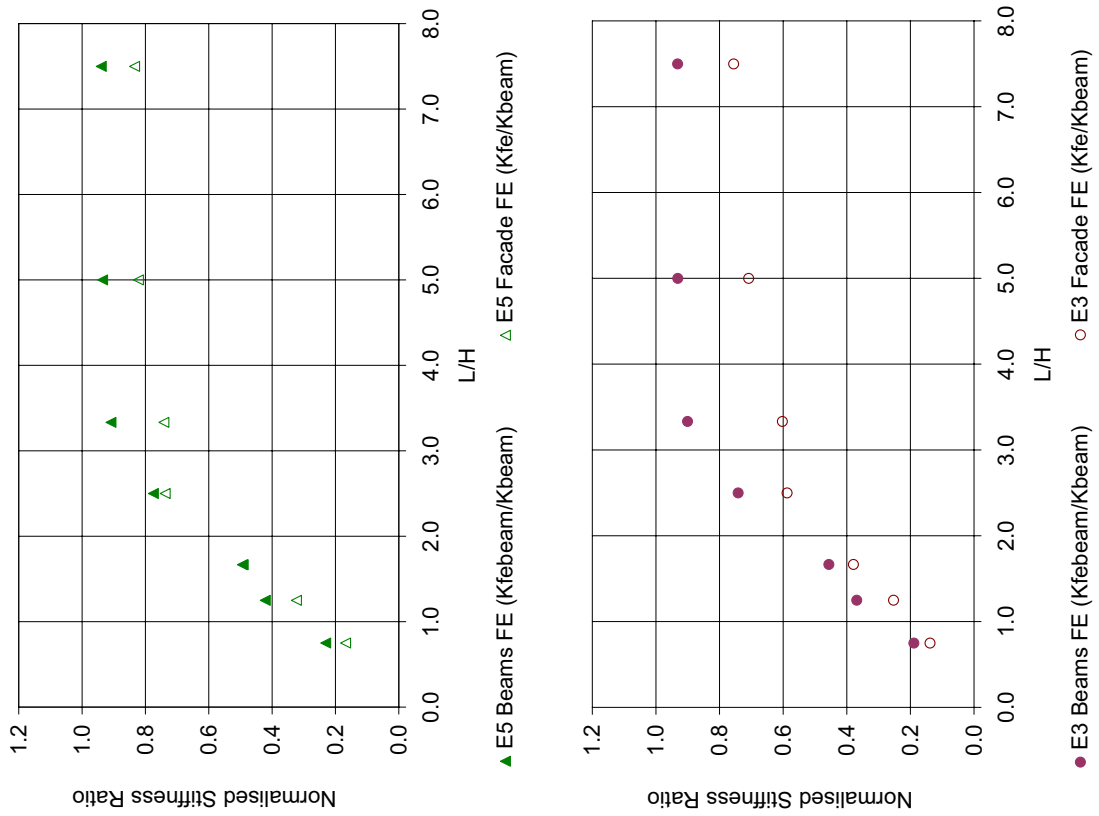

(c) Models E5 - 9.375% Windows

(d) Models E3 - 18.750% Windows

Figure 6.9: **Observed finite element Beam and Facade response to applied displacement (smooth based)**

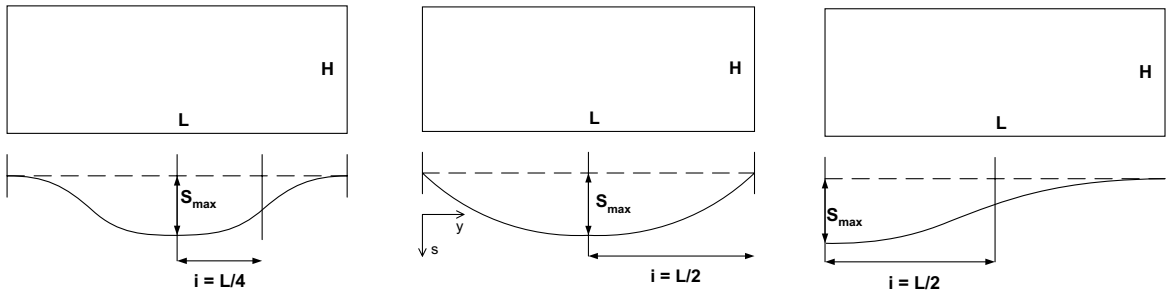

(a) 1. Symmetrical 1: i=L/4 (b) 2. Symmetrical 2: i=L/2 (c) 3. Asymmetrical: i=L/2

Figure 6.10: **Gaussian applied displacements**

reasonably well. Such a conclusion, however, is to be expected as method to assign the beam properties was developed based on identical analyses to those described above. It is therefore desirable to test the beams under a different set of displacements.

6.6.2 Beams and facades with Gaussian displacement

To ensure that the Timoshenko beam formulation and equivalent elastic beam properties are robust, a series of finite element analyses is undertaken where Gaussian displacements are applied to the beams and the full facades. A Gaussian displacement profile is the classic profile assumed to describe the surface settlement trough arising from tunnelling at a greenfield site as described in section 2.2. The equation for vertical settlement is given as equation 2.1. The magnitude of the maximum vertical settlement chosen is S_{max}=0.01m. For these analyses three different Gaussian displacement profiles are applied by varying the position and size of the building relative to the tunnel as shown in figure 6.10. These displacements are applied to the $20 \times 8m$ facades denoted A13 (no openings) and A33 (18.75% openings) and beams representing these facades.

The results are as shown in figure 6.11. The results show the stress at the same nodal locations for the facades and the beams and indicate that the beams respond to the applied displacements in an acceptably similar manner. The jagged nature of the response of the facades with windows can be seen to be smoothed by the beams. Another difference is that while all the tests show good agreement between the beam and the facade results in the middle of the facade, the beams all exhibit larger stresses at the end points. This is

thought to be due to difference in dimensionality between the beams (1D line elements), and the facades (2D planes) with stresses throughout the whole facade.

6.7 Conclusion

Timoshenko beams have been formulated and implemented successfully into the OXFEM finite element program. Two constitutive models have been implemented for the beam elements: an elastic model and a non-linear no hogging model. The beam elements have been tested and the response of the beams to simple applied displacements has been compared favourably to the response of full facades. While useful for confirming the robustness of the beam implementation and the new equivalent elastic and masonry beam models, the simple applied displacement approach is merely a pre-cursor to the main focus of this research: the use of beam elements to represent masonry buildings in three-dimensional numerical models of tunnel construction. It is on this problem that the remaining chapters of this thesis concentrate.

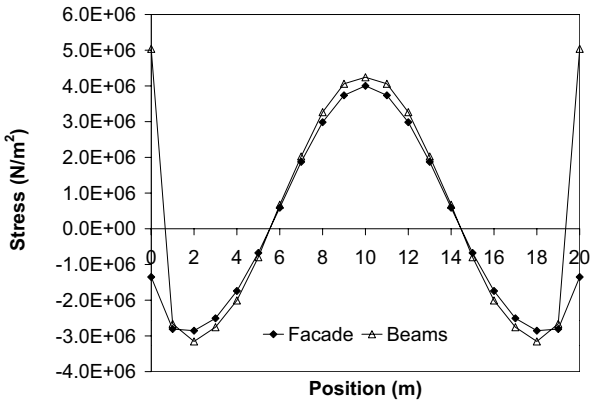

(a) E13 Gauss Disp.1

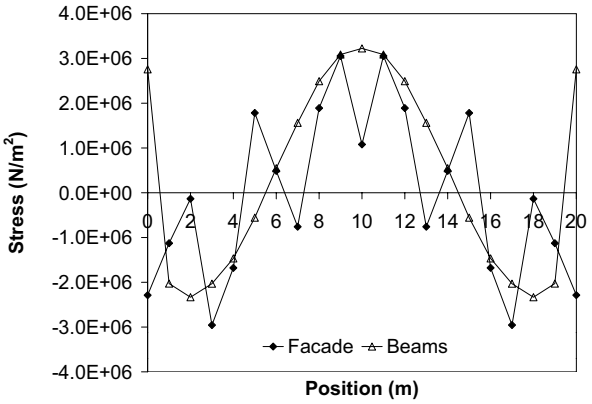

(b) E33 Gauss Disp.1

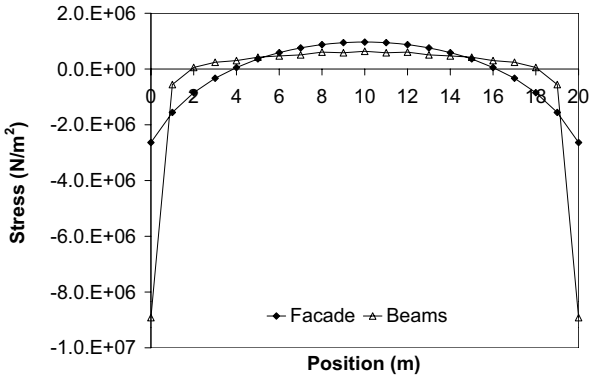

(c) E13 Gauss Disp.2

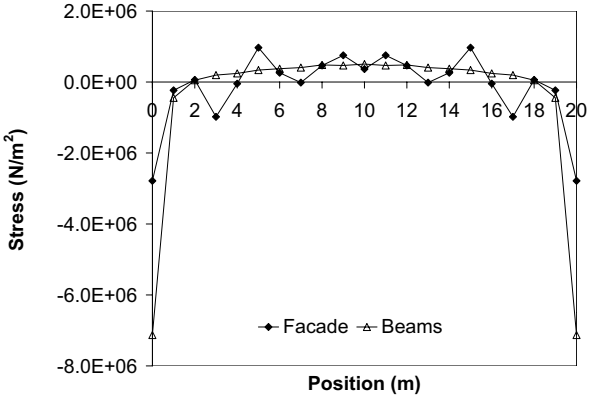

(d) E33 Gauss Disp.2

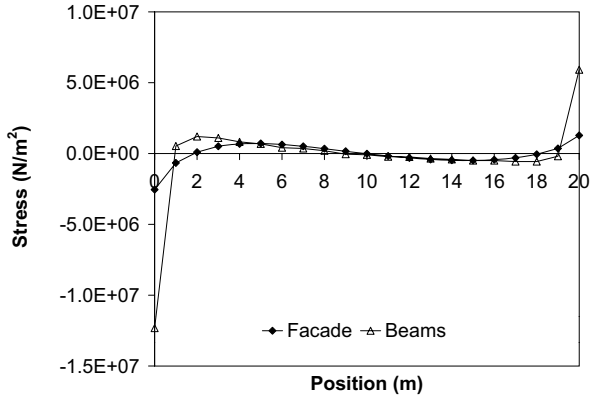

(e) E13 Gauss Disp.3

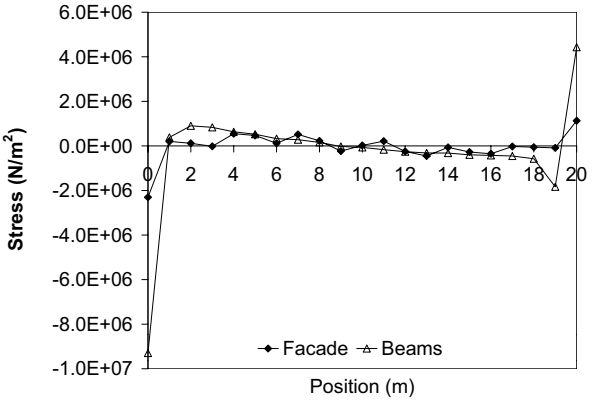

(f) E33 Gauss Disp.3

Figure 6.11: **Facades E13 (no windows) and E33 (18.75% windows) and equivalent beam response to imposed Gaussian displacements (from figure 6.10)**

Chapter 7

Composition of three-dimensional numerical model

7.1 Introduction

This chapter describes the composition of three-dimensional numerical models for analysis of building response to tunnelling. The procedure for mesh generation, the constitutive models used and the solution technique employed are outlined along with a description of the use of shared memory parallel computing. The numerical simulation of the tunnelling process is described. The computational task for all the three-dimensional analyses was performed using the Oxford in-house finite element software OXFEM.

7.2 Mesh generation and pre-processing

The pre-processing tasks necessary to prepare a three-dimensional numerical model for analysis in the OXFEM finite element program are similar for all the numerical models analysed in this thesis. They include geometric wire frame modelling, mesh generation, and production of the OXFEM input file.

Geometric modelling and mesh generation for all three-dimensional problems was under-

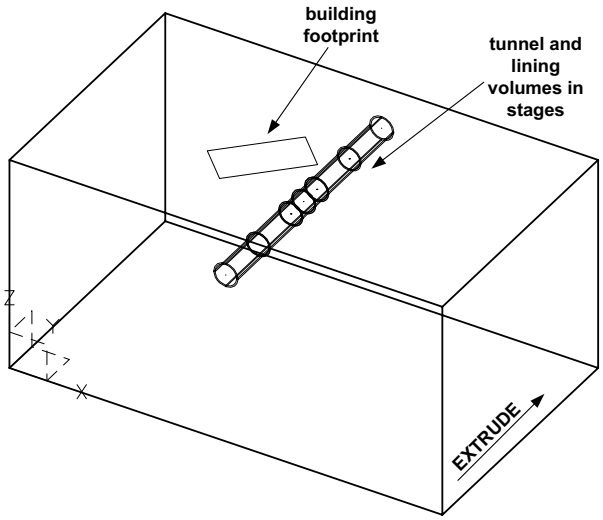

Figure 7.1: **Wire frame model with tunnel stages and building footprint**

taken using the *modelling* module within the I-DEAS software described in Chapter 4 (in relation to the 2D work). The generation of a model, following the initial choice of geometric layout, commences with wire frame modelling of the soil and tunnel. The face of the soil block is drawn on a vertical plane and is then extruded in the direction of tunnelling to create a 3D block of soil. Building footprints are drawn on the soil surface. The cross section of the tunnel and its lining is then drawn on the soil face and extruded through the soil progressively to create partitioned volumes corresponding to the desired sequential tunnelling stages. Figure 7.1 illustrates this process, showing the wire frame generated for a tunnel with six construction stages under a building oblique to the tunnel alignment.

Once the wireframe model is complete, each region within the model is meshed using the I-DEAS *meshing* module. Element lengths are refined so that areas of local interest, such as the building footprint and the tunnel, have smaller elements than remote areas. Such an approach aims to strike a balance between an appropriate level of detail in areas of interest and the minimisation of the total number of degrees of freedom in the model.

Elements used for the soil and tunnel lining are 10-noded tetrahedral elements. These are chosen as it is considered that for modelling incompressible, undrained material behaviour in three dimensions using exact integration, the tetrahedron family of elements is superior to both the serendipity and Lagrangian cube families (Bell et al., 1991). 20-noded tetrahedral elements are considered to be the most suitable tetrahedral element type. Fewer

20-noded elements than 10-noded ones are required to model a problem with a similar level of accuracy. Problems with complex geometries, such as those for this thesis with tunnels and building footprints can require a large number of small elements. Modelled with 20-noded elements, such problems can have very large numbers of degrees of freedom, however, leading to computational inefficiency. For the analyses in this thesis, therefore, 10-noded tetrahedral elements are used for the soil as they are computationally more efficient while still being suitable for modelling incompressible material. The choice of elements for the tunnel lining is discussed in detail below.

Node positions known as *anchor nodes* in I-DEAS are defined around the building footprint allowing the building mesh, which is generated separately, to be added later and matched to the soil. Groups of elements such as the tunnel lining and the tunnel interior elements which are to be excavated at each stage are defined in I-DEAS for later use in the OXFEM input file. Groups of nodes such as all those on the surface or around the building footprint, are also defined to facilitate results output and post-processing.

The final task within I-DEAS is to check the mesh for any errors. Checks for multiple nodes or zero volume elements are simple to carry out and any duplicated or erroneous elements and nodes are removed. Checks can also be performed to ensure that elements do not have poor geometric conditioning which could lead to errors during calculation. Of particular concern are the elements comprising the tunnel lining, which, for the analyses in this thesis, consist of continuum elements as discussed below. A check for geometric conditioning successfully used by Wisser (2002) is the stretch, ζ, of an element where

$$\zeta = \sqrt{24} \times \frac{\text{radius of the largest circle that will fit inside the element}}{\text{longest edge of an element}} \tag{7.1}$$

The minimum stretch suggested for acceptable geometric conditioning by I-DEAS is 0.05, however as Wisser notes, this value should be only considered as a guideline, as the appropriate value will depend on the problem analysed and the location of each element within the mesh. In addition, it is considered that any round-off errors associated with thin elements with poor geometric conditioning are insignificant as the calculations are undertaken

using double precision arithmetic.

The meshed model file is exported from I-DEAS into the ABAQUS commercial software format and is then converted into a format readable by OXFEM using a FORTRAN program written by Augarde (1997) as amended by Bloodworth (2002) called CONVERT5.

For analyses including a building, the meshes for the facades, consisting of six-noded plane stress triangular elements, are generated separately in I-DEAS and exported and converted to OXFEM format using the CONVERT FACADE program described in Chapter 4. The building information is then added to the soil input file. To connect the building facades, which are defined in local two-dimensional coordinate systems, to each other and to the soil block (defined in three dimensions), tie elements developed by Liu (1997) are used. Previously these tie elements were generated during an OXFEM run. This facility has been separated as part of this project as this pre-processing utility is not a core operation of the analysis program. A new program, TIE-GEN, now generates these tie elements.

The OXFEM input file is completed by adding material parameters, instructions for the staged tunnel construction and output requirements. Timoshenko beam elements for analyses where the building is represented by surface beams are also added at this stage.

7.3 Simulation of tunnelling

Numerical simulation of tunnel construction requires the modelling of three main activities: soil excavation, lining installation and volume loss generation. A range of techniques to simulate these three activities is discussed in section 2.3.2. In this thesis, the tunnel is constructed in a number of stages to simulate passage in the longitudinal direction under a building or buildings of interest. For each tunnel construction stage, modelling of soil excavation is achieved by the removal from the overall mesh of elements representing the interior of the tunnel and the imposition of nodal loads on the excavated boundary to remove surface tractions according to the method of Brown and Booker (1985).

Techniques used in this thesis for the modelling of tunnel lining and volume loss build on

Table 7.1: **Material properties for concrete tunnel lining**

G	ν	γ	s_u
1.25×10^7kPa	0.2	20.0kPa/m	1.0×10^6kPa

previous work at the Oxford University. Augarde (1997) introduced the use of overlapping shell elements for modelling lining in three dimensions. Subsequently, Augarde and Burd (2001) and Wisser (2002) compared the use of these shell elements with the use of continuum lining elements. They concluded that despite the possibility of sub-optimal geometric conditioning of thin continuum elements in the lining (discussed above), surface settlement results due to a tunnel lined with continuum elements were smoother than with a shell element lining. Continuum lining elements are thus used for all tunnelling analyses in this thesis. Wisser (2002) also investigated the modelling of face support during tunnelling operations and concluded that face support is only necessary in analyses involving very soft ground; in stiffer soil the application of face support did not have a significant influence on the settlement profile and it is thus not applied during the analyses in this thesis.

The tunnel construction process is modelled as follows: at the start of an analysis, all elements in the soil block, including those representing the the interior of the tunnel and the lining, are soil elements. At each tunnel construction stage, the material properties of the lining elements are switched from soil to concrete. Linear elastic material properties are assumed for the concrete and the properties for the lining in all analyses in this thesis are given in table 7.1. The soil elements in the tunnel are then excavated.

Volume loss is modelled by the application of a uniform shrinkage to the tunnel lining. This is achieved by the application of nodal forces to the nodes in the lining elements (Wisser, 2002). The nodal load vector, $\boldsymbol{f_e}$, for each lining element is given by

$$\boldsymbol{f_e} = \boldsymbol{K_e}\, \boldsymbol{d_e} \tag{7.2}$$

where $\boldsymbol{K_e}$ is the element stiffness matrix and $\boldsymbol{d_e}$ is the element nodal displacement vector

comprising the displacement vectors of each node such that

$$\boldsymbol{d_e}^T = [\boldsymbol{d_1}\ \boldsymbol{d_2}\ \ldots\ \boldsymbol{d_{10}}] \tag{7.3}$$

The displacement vector of node i is calculated by

$$\boldsymbol{d_i} = \delta_r \frac{\boldsymbol{n_i}}{|\boldsymbol{n_i}|} \tag{7.4}$$

where $\boldsymbol{n_i}$ is the vector perpendicular to the tunnel axis pointing from node i to the tunnel axis and δ_r is the required radial displacement.

The method of tunnel construction simulation outlined above can be considered as an 'outcome driven' method as the desired volume loss for the analysis is directly applied within the model. This differs from the alternative approach where the analyst attempts to model the exact tunnelling process that causes the volume loss. As described in Chapter 2, both these general approaches have been followed in numerical analyses reported in the literature. The outcome driven approach, as well as being simpler to implement, is more suitable to modelling situations where the volume loss is known in advance such as back-analyses or Class B or C predictions (i.e. during or after the event (Lambe, 1973)). In addition, the outcome driven approach is considered by some (Lee and Rowe, 1990a) to be more robust even for Class A predictions (before the event). This is due to the assertion that even if one is able to exactly model the tunnelling process, it is not possible to model the human factor in tunnelling operations. For example, during real construction the use of the same tunnelling machine may lead to different volume losses when operated by different crew; a well-trained, experienced tunnelling crew may operate the machine more accurately resulting in less volume loss than an inexperienced poorly trained crew.

7.4 Soil model

A discussion regarding the range of constitutive models used for soil in finite element analyses is given in section 2.3.2. This concluded with noting the importance of modelling

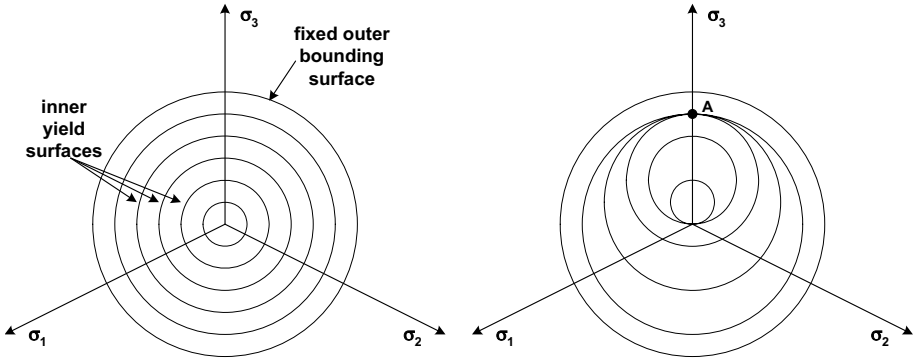

Figure 7.2: **Nested yield surface model for soil (after Houlsby, 1999)**

the small strain non-linearity of soil when assessing the effects of ground movements due to tunnelling. For the tunnelling analyses in this thesis the nested yield surface model by Houlsby (1999) is used which models the non-linearity of a clay soil at small strains. This model consists of a number of nested yield surfaces within an outer fixed von Mises surface. The model is a kinematic work hardening plasticity model in which the inner yield surfaces translate as plastic strain occurs. As a stress point moves in space and encounters a yield surface, the stiffness reduces and the yield surface moves with the stress point. The model thus simulates the non-linearity of response at small strains and the effect of recent stress history. Figure 7.2 illustrates the model in its initial state and for an example situation where with the yield surfaces have translated after a stress point moves from the origin to point A and back again.

Each nested yield surface is described by parameters defining its size and the amount of stiffness reduction as the yield surface is reached. The tangential shear stiffness, G_i, after yield surface i has been reached is

$$G_i = g'_\alpha \times G_0 \tag{7.5}$$

where g'_α is a parameter describing the decrease in shear stiffness at an inner yield surface and G_0 is the shear modulus. The triaxial yield strength, c_i, for yield surface i is

$$c_i = c'_\alpha \times c \tag{7.6}$$

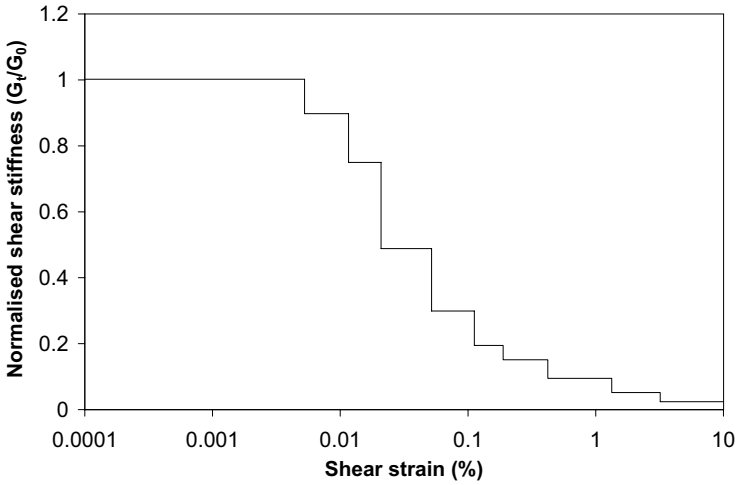

Figure 7.3: **Tangent shear stiffness variation with strain for nested yield surface model**

where c is the undrained shear strength of the material $c = 2s_u/\sqrt{3}$, s_u is the undrained strength in triaxial compression and c'_α is a parameter governing the size of the particular inner yield surface. The outermost yield surface is fixed and defines the undrained shear strength of the material.

The stiffness response of soil under this model is illustrated in figure 7.3 which shows the change in tangent shear modulus of the soil with shear strain. Parameters used to plot this figure are those chosen as typical for London clay by Houlsby (1999).

The soil model allows for the undrained shear strength and shear modulus to increase with depth. The shear modulus at any depth, z, below the surface is given by

$$G_0 = G_0^s + \omega z \tag{7.7}$$

where G_0^s is the shear modulus at the surface and ω is the increase in shear modulus per metre depth. The undrained shear strength at depth z is

$$s_u = s_{u0} + \mu z \tag{7.8}$$

where s_{u0} is the undrained shear strength at the surface and μ is the increase in strength with depth.

The parameters required to fully define the model are thus:

- initial shear modulus at the surface inside the first yield surface, G_0^s
- undrained shear strength at surface, s_{u0}
- increase in s_u with depth, μ
- increase in G_0 with depth, ω
- unit weight, γ
- Poisson's ratio, ν
- n pairs of constants describing the n inner nested yield surfaces, c'_α, g'_α

The values used for each of the parameters above are given with the description of each analysis in Chapters 8 and 9.

7.5 Solution technique and calculation process

The solution of a finite element problem involves the solution of the set of equations

$$\boldsymbol{K}\,\boldsymbol{d} = \boldsymbol{f} \tag{7.9}$$

where $\boldsymbol{d}$ comprises the displacements at the nodal degrees of freedom, $\boldsymbol{K}$ is the stiffness matrix and $\boldsymbol{f}$ comprises the nodal forces. The method used for this task in OXFEM is a Frontal solution method based on Gaussian elimination. In a Frontal solver, the full global stiffness matrix is never fully assembled; the assembly process is interrupted at intervals when there are enough complete rows and columns in the stiffness matrix to perform the reduction by Gaussian elimination of complete columns (Astley, 1992). Entries in the stiffness matrix are complete when they will receive no more contributions from any other degrees of freedom. Entries may also be empty, having received none of their contributions or partially complete, having received some but not all. The empty and partially complete

terms comprise the active portion of the stiffness matrix; the complete terms having been stored separately for back-substitution. The instantaneous size of the active portion of the matrix is known as the frontwidth and it is in the interest of the engineer to keep this to a minimum. The frontwidth is dependent on the order in which elements are handled by the solver. Efficient solutions to finite element problems thus involve the re-ordering of the element numbers prior to solution to minimise the frontwidth and thus the solution time. The optimisation program OXOPT written by Prof. Guy Houlsby, based on the algorithm by Sloan and Randolph (1983) is used for for this task having been successfully used for previous numerical modelling research (Wisser, 2002; Bloodworth, 2002; Augarde, 1997; and Liu, 1997).

The stiffness matrix for a non-linear material such as the no-tension masonry or the nested yield surface soil, depends on the current stress level. For the solution of such problems alternatives include an iterative approach such as the Newton-Raphson method or an incremental approach such as a modified Euler scheme (Cook et al., 1989). Both methods are available in OXFEM, with the Newton-Raphson solution scheme having been implemented as part of concurrent but unrelated research. For all analyses in this thesis, the modified Euler scheme is used with loading applied over a number of steps and the out-of-balance between the equilibrium force at the current stress level and the original applied force applied as a correction at the next step (Burd, 1986).

7.6 Shared memory parallel computing

Large three-dimensional finite element analyses can suffer from long run times, particularly when non-linear material models are used. The use of parallel computing significantly reduces the calculation time for large finite element analyses. Parallel computing involves the partitioning of time consuming calculations and the distribution of these to a number of different individual processors where independent calculations are computed in parallel, reducing the run time compared to a serial calculation (Graham, 1999). This reduction in run times is particularly useful for research where a large number of slightly different runs

of the same problem may need to be performed, for example in parametric studies

There are two main types of parallel computing: distributed memory and shared memory systems. In a distributed memory system, each processor has its own local memory with processors linked together able to distribute information by message passing. A shared memory system consists of a number of processors all with access to a global memory store, meaning that each processor does not have its own memory (except for a small cache) but each has the same view of all memory globally. Communication between processors is by one processor writing data to the global memory and another reading those data; there is no need for direct communication between processors (McLatchie et al., 2003). Hybrid systems (also known as shared distributed systems) also exist, where each processor has its own memory as in a distributed system, but in addition, all processors can view each other's memory. The main advantage of a shared memory system for programming and use is that there are no explicit communications between processors, simplifying programming and use. Two shared memory systems were used for this project.

The first shared memory system used for this project was the OSWELL system at the Oxford Supercomputing Centre (OSC). The OSWELL system consisted of 84 processors in four partitions comprising 24; 24; 12; and 24 processors with 48; 48; 24; and 48Gbytes of memory in each partition respectively, giving a total of 168Gbytes. A job ran within one partition such that a maximum of 24 processors could be used, although typically users request less than the full complement of processors in a partition for a job. Each of the 84 processors was a Sun Fire 6800 UltraSparc III 900MHz machine. User access to the system was through a head node comprising two Sun Fire V880 750MHz machines with 4Gbytes RAM and the use of a Sun GridEngine 5.3p2 job scheduling queue system (McLatchie et al., 2003).

The second shared memory system used for this project was the KONRAD system which replaced the OSWELL system at the OSC from August 2005. KONRAD consists of 24 processors; eight on each of three compute nodes with each node sharing 32Gbytes of memory. Each processor is a Dual-Core AMD Opteron 865 1.8GHz machine. The head node for the system is a Dual AMD Opteron 246 2.0GHz machine with 4Gbytes DDR, and

uses a Sun GridEngine scheduler.

For use in parallel computing the original FORTRAN90 code for OXFEM was parallelised. The method employed for this task was the use of the OpenMP standard for shared memory systems. Using OpenMP to parallelise existing serial code such as OXFEM involves inserting new OpenMP compiler directives into the code to indicate regions to be executed in parallel and give details about the parallelisation (Graham, 1999). Regions of the code parallelised generally include only the more time consuming operations. A significant advantage of the OpenMP standard is that the directives appear as comments to a serial compiler but operative code to a parallel compiler, allowing the same versions of the program to be maintained for both serial and parallel computing.

Although the OXFEM code was already parallelised prior to the start of this project, an older supercomputer (the OSC system known as OSCAR; a hybrid shared distributed system) was used previously. OSWELL, having been installed at the OSC in 2002, replaced OSCAR necessitating the the migration of the OXFEM code to the new system from the local civil engineering group network where the program is run in serial. This task involved the migration, parallel compilation and testing of the code on the new OSWELL system. This provided an opportunity for an upgrade of a number of sections of the code, facilitated by the more rigorous compilers on the supercomputer. This process of migrating the OXFEM code, compiling and testing was repeated when the KONRAD system replaced OSWELL.

The use of the supercomputer was beneficial in minimising run times for this project. Typical run times for analyses with approximately 13,000 degrees of freedom and 110 calculation steps used to take as long as 180 hours (approximately 8 days) to run in serial on the fastest civil engineering network machine at the time, a Sun 400MHz, 512Mbyte machine under UNIX. The use of the OSCAR supercomputer reduced such analyses to approximately five hours with eight parallel processors employed (Bloodworth, 2002). On OSWELL, during the current project, analyses with approximately 30,000 degrees of freedom and 115 calculation steps took around eight hours to run with eight parallel processors.